First-principle investigation on perovskite $La_{1-x}Eu_xGaO_3$*

Yanni Gu(顾艳妮)[1,2], Sheng Xu(徐胜)[1,2], and Xiaoshan Wu(吴小山)[1,†]

[1] *Laboratory of Solid State Microstructures and School of Physics, Nanjing University, Nanjing* 210093, *China*
[2] *Zhangjiagang Campus, Jiangsu University of Science and Technology, Zhangjiagang* 215600, *China*

(Received 7 July 2016; revised manuscript received 28 August 2016; published online 25 October 2016)

The pseudopotential method has been used to investigate the structural, electronic and magnetic properties of $La_{1-x}Eu_xGaO_3$ ($x = 0$, 0.25, 0.5, 0.75, and 1) within the scheme of generalized gradient approximation. The spin-polarized calculations demonstrate that the ground state is an antiferromagnetic insulator for $x \leq 0.5$, while it is ferromagnetic half-metal at $x > 0.5$. The substitutions of magnetic Eu ions for non-magnetic La ions produce and strength spin polarization, which forcefully urges the system from the insulator to the half metal. Meanwhile, Eu doping strengthens a stoner mechanism for ferromagnetism of $La_{1-x}Eu_xGaO_3$ ($x = 0.75$ and 1), which may lead to a rapid increasing in the total magnetic moment and therefore, antiferromagnetic–ferromagnetic transition happens.

Keywords: spin-polarized calculations, electronic and magnetic properties, Eu-doped Prevskite $LaGaO_3$

PACS: 31.15.ej, 31.15.ae, 75.30.Hx **DOI:** 10.1088/1674-1056/25/12/123103

1. Introduction

Many researchers persistently focus substantial concern on orthogallates due to their particular physical properties and promising applications in devices. $LaGaO_3$ is one of these compositions. It is the most suitable compound for interconnecting material in solid oxide fuel cells (SOFC).[1–5] Aside from possible applications for electrolyte of solid fuel, $LaGaO_3$ has many other potential applications, such as luminescence and thermal potential.[6–10]

At room temperature, $LaGaO_3$ crystal has an ABO_3 perovskite structure with $GdFeO_3$-type distortion and falls into the orthorhombical space group *Pbnm*.[11] GaO_6 octahedra are not aligned along the unit-cell axes. Lanthanide ions doping on A-sites have significant effects on the structural and physical properties of $LaGaO_3$. Liu *et al.*[6–9] reported Ln^{3+}-doped (Ln = Eu, Dy, Tm, Tb, Sm, and Tb) $LaGaO_3$ nanocrystalline phosphors, investigating the crystallization process, photoluminescence, and cathodoluminescence properties. Parveen *et al.* have studied the thermal properties of $La_{1-x}Ln_xGaO_3$ (Ln = La, Ce, Nd, Pr).[10] Sood *et al.* studied structural and electronic behavior of Ba-doped $LaGaO_3$.[12]

Most of these researches are focused experimentally on the photoluminescence, cathodoluminescence and thermal properties, etc., while there is almost no theoretical work on electronic structure and magnetic property for Ln^{3+}-doped $LaGaO_3$ (Ln = rare earth elements) although there are some first-principle researches about effects of doping on physical properties of other systems within density-functional theory.[13–17] Theory research has important instruction significance for experimental work.

Here, the investigation of structural, electronic, and magnetic properties for $La_{1-x}Eu_xGaO_3$ ($0 \leq x \leq 1$) are carried out using the generalized gradient approximation (GGA). The unit cell stability, the electronic structure, and the magnetic structure are determined. The further experiments are needed to confirm the present transition of $La_{1-x}Eu_xGaO_3$ from antiferromagnetic (AFM) insulator to ferromagnetic (FM) half metal.

2. Computational details

We performed the first-principle calculations of $La_{1-x}Eu_xGaO_3$ ($x = 0$, 0.25, 0.5, 0.75, and 1) using the GGA method and the projector-augmented wave (PAW)[18] potentials, which are implemented in the Vienna *ab initio* Simulation Package (VASP)[19,20] program. In order to study the structural, electronic and magnetic properties of $La_{1-x}Eu_xGaO_3$, a supercell has been constructed consisting of 40 atoms with size $\sqrt{2}a \times \sqrt{2}b \times c$, as shown in Fig. 1. Every possible substituted site and magnetic configuration of $La_{1-x}Eu_xGaO_3$ was taken into account and the total energy was assessed for each test structure. We optimized atomic coordinates and axial ratios for each test structure during the simulations. The Hellman–Feynman forces are converged to less than 1 meV/Å and the energy difference of two successive iterations is less than 1×10^{-6} eV/cell. The plane-wave energy cutoff for the electrons is 500 eV and a $7 \times 7 \times 7$ grid of Monkhorst–Pack mesh is used for the k-point sampling. The structure with the lowest total energy is regarded as the ground state structure. We replaced La_2 and La_6 atoms by Eu atoms

*Project supported by the National Natural Science Foundation of China (Grant Nos. U1332205, 11274153, 10974081, and 10979017) and the Postdoctoral Fund of Jiangsu Province, China (Grant No. 1301019B).

†Corresponding author. E-mail: xswu@nju.edu.cn

© 2016 Chinese Physical Society and IOP Publishing Ltd

for the $x = 0.25$ lattice (Fig. 1), La_2, La_3, La_6, and La_7 atoms for $x = 0.5$, and La_2, La_3, La_4, La_6, La_7, and La_8 atoms for $x = 0.75$, respectively. The replaced structure has the lowest total energy.

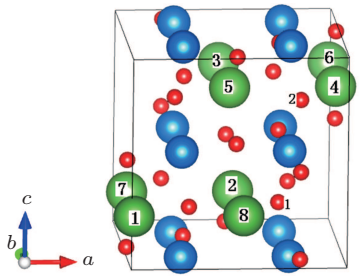


Fig. 1. (color online) A 40-atom supercell of perovskite structure $LaGaO_3$. The green, blue, and red spheres represent La, Ga, and O atoms, respectively. Eight different sites of La atoms and two O atoms are marked with arabic numerals.

3. Results and discussion

3.1. Structure relaxation

The calculated structural parameters for different compositions are given in Table 1. We optimize the unit cell symmetry, lattice constants, and atomic coordinates simultaneously. The crystal structure of $La_{1-x}Eu_xGaO_3$ falls into the space group *Pbnm* ($x = 0$ and 1) or $P21/m$ ($x = 0.25$, 0.5, and 0.75). We determine the space groups using the FINDSYM program.[21] It is well known that the volume may be overestimated for 2%–3% with the GGA method.[22] The cell volume for $LaGaO_3$ is 243.67343 Å, and $EuGaO_3$ is 232.36297 Å (see Table 1). The calculated lattice parameters and space group in the two parent compounds $LaGaO_3$ and $EuGaO_3$ are in reasonable agreement with experimental results.[23–27]

Table 1. Calculated structural parameters and total magnetic moments for $La_{1-x}Eu_xGaO_3$ ($x = 0$, 0.25, 0.5, 0.75, 1).

Composition x	0	0.25	0.5	0.75	1
Space group	*Pbnm*(62)	$P21/m$(11)	$P21/m$(11)	$P21/m$(11)	*Pbnm*(62)
a/Å	5.58051	5.57158	5.53877	5.50303	5.42866
b/Å	5.56049	5.54833	5.54825	5.53730	5.52864
c/Å	7.85274	7.85538	7.82058	7.76244	7.74205
V/Å^3	243.67343	242.83308	240.33018	236.5365	232.36297
d (Eu_1–O_1)/Å	0	2.38908	2.37274	2.35423	2.34054
d (La_5–O_2)/Å	3.19008	3.18776	3.17279	3.15293	0
$\mu_T/(\mu_B$/f.u.)	0	0	0	4.48400	5.97775

The cell volume, bond distances $d_{(Eu_1-O_1)}$ and $d_{(La_5-O_2)}$ decrease linearly with the increasing Eu composition x, as shown in Fig. 2. It can be understood by Vegard law[28] since the ionic radius of Eu^{3+} (0.95 Å) is smaller than that of La^{3+} (1.06 Å).

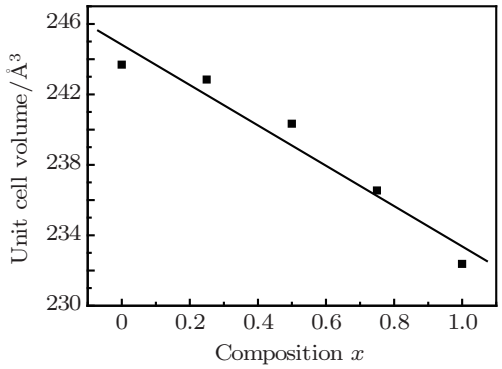


Fig. 2. The composition x dependence of calculated unit cell volume V in $La_{1-x}Eu_xGaO_3$.

3.2. Electronic structure

The GGA calculation results show that the electronic ground states of this system are insulators when $x \leq 0.5$, and are half-metals for $x > 0.5$. The calculated total density of states (TDOS) of $La_{1-x}Eu_xGaO_3$ and partial Eu, Ga, O, and La atomic projected DOS (PDOS) for different contents are shown in Fig. 3. Band decomposed charge density plots are shown in Fig. 4. The DOS under our considerations is limited to an energy window of −9 eV to 8 eV, and we focus mainly on the La 4f, Eu 4f, and O 2p orbitals because the value and conduction bands of $La_{1-x}Eu_xGaO_3$ do not derive from Ga states.

$LaGaO_3$ is known as an insulator, which corresponds with our DOS calculation (see Fig. 3(a)). The O 2p bands are situated at −7.5 eV and −0.3 eV, and La 4f bands cross from 3.89 eV to 4.80 eV. The valence band is dominated by O 2p π orbitals and the conduction band is composed mainly by hybrid La 4f orbitals, as shown in Figs. 4(a) and 4(b). The energy gap is around 4.19 eV in agreement with the theoretical result.[29]

For $x = 0.25$ in $La_{1-x}Eu_xGaO_3$ (see Fig. 3(b)), the primary peaks of spin-up and spin-down of O 2p orbitals are situated from −6.5 eV to 0.21 eV. Eu 4f bands are from −1.32 eV to 0.30 eV and from 3.82 eV to 4.55 eV, separately. As shown in Figs. 4(c) and 4(d), the valence bands consist of O 2p π orbitals and Eu 4f δ orbitals, and the conduction band is composed chiefly of Eu 4f π orbitals, generating an insulator ground state with energy gaps of 3.52 eV.

For $x = 0.5$ (see Fig. 3(c) and Figs. 4(e) and 4(f)), the valence band is dominated by O 2p orbitals and Eu 4f orbitals. The conduction band is dominated by Eu 4f orbitals. There is an energy gap of 3.35 eV between the valence band top and conduction band bottom resulting in an insulating ground state. Figures 3(b) and 3(c) both have symmetrical DOS between spin-up and spin-down bands since the ground states of these compounds are AFM (see Table 2).

With further increasing of Eu concentration, the DOS of the compounds change inevitably. For $x = 0.75$ (see Fig. 3(d) and Fig. 4(g)), the spin-up valence bands crossing the Fermi level are dominated by the admixture of Eu 4f, and O 2p states, while the spin-down valence bands are mainly composed of O 2p states below the Fermi level E_F. Therefore, the general characteristics of the DOS for the $x = 0.75$ sample show a half-metal FM ground state character. Occupied Eu 4f states are considerably narrow and sharp, indicating that they are localized states.

Finally, our calculation results demonstrate that $EuGaO_3$, i.e., the compound $x = 1$ (see Fig. 3(e), has a half-metal FM ground state. The O 2p bands cross the Fermi surface from -6.5 eV to 0.46 eV, while the main peaks of spin-up Eu 4f bands are located from 1.71 eV below to 0.46 eV and spin-down at 3.7 eV, respectively. The spin-up bands of $EuGaO_3$ straddle the Fermi level, while the spin-down are totally below Fermi level, resulting in a half-metallic FM ground state. As shown in Fig. 4(h), the bands near Fermi level are dominated by O 2p states and Eu 4f states.

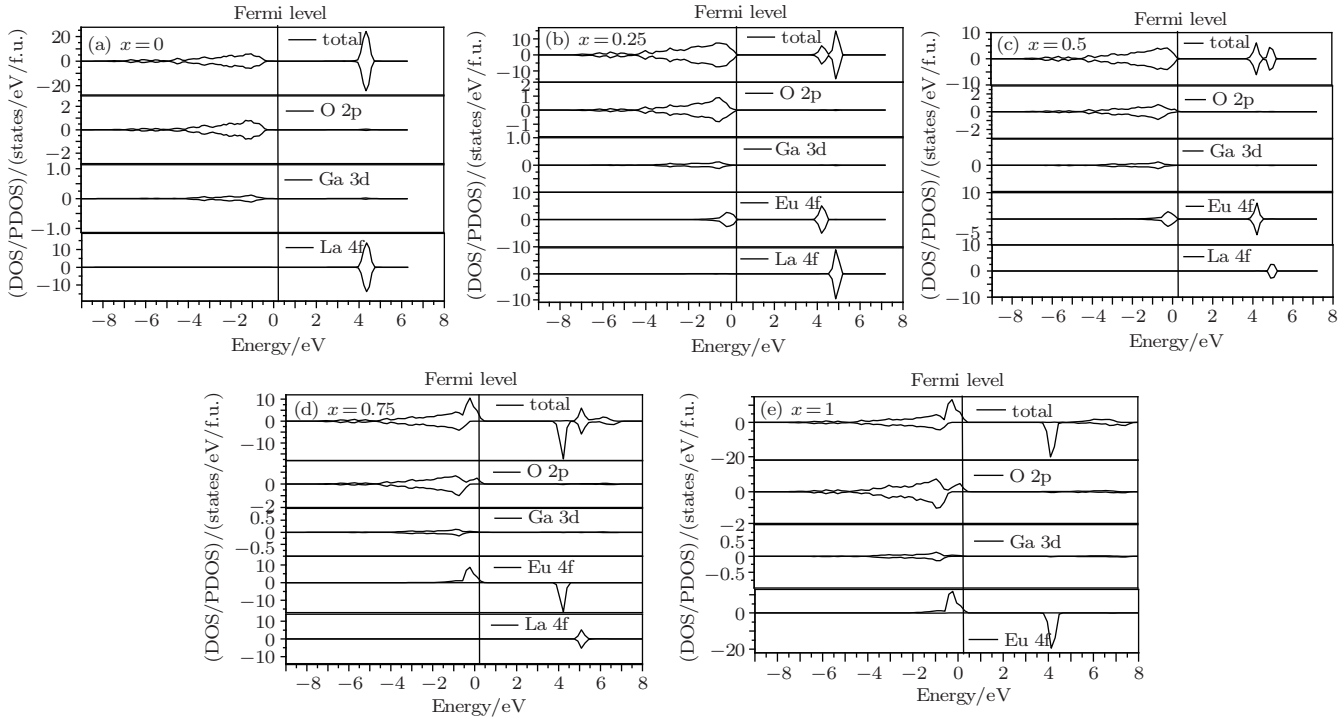


Fig. 3. The total DOS and projected DOS of $La_{1-x}Eu_xGaO_3$ ($x = 0$, 0.25, 0.5, 0.75, 1). Fermi levels are black vertical lines in the figure.

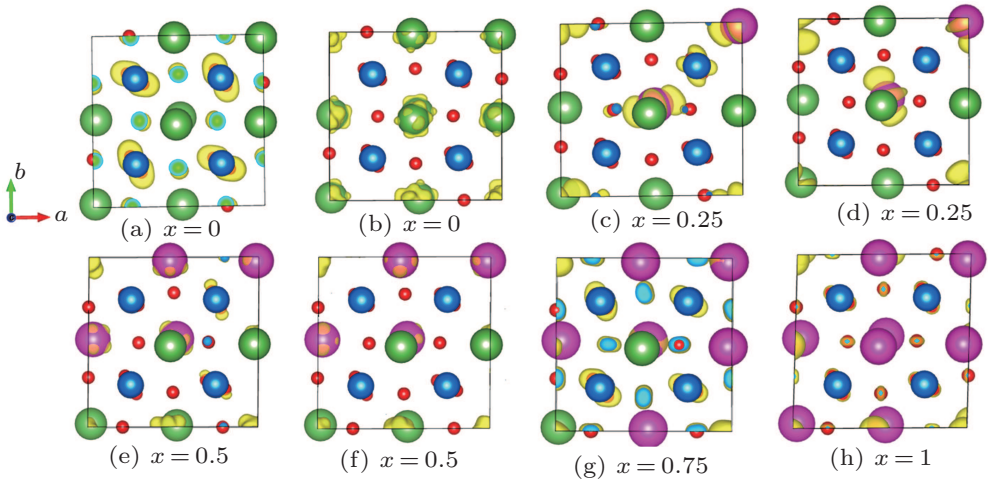


Fig. 4. (color online) Band decomposed charge density of (a) value band at $x = 0$, (b) conduction band at $x = 0$, (c) value band at $x = 0.25$, (d) conduction band at $x = 0.25$, (e) value band at $x = 0.5$, (f) conduction band at $x = 0.5$, (g) bands near Fermi level at $x = 0.75$, and (h) bands near Fermi level at $x = 1$. We show the bands near Fermi level at $x = 0.75$ and $x = 1$ because these materials are half-metal according to the present results.

In summary, DOS and PDOS of $LaGaO_3$ are symmetric between spin-up and spin-down bands as shown in Fig. 3(a), and therefore the magnetic moment is zero. There is an energy gap of 4.19 eV for $LaGaO_3$, which generates an insulating ground state. In Figs. 3(b) and 3(c), non-magnetic La ions are substituted by localized magnetic Eu ions. DOS shows the symmetrical behavior between spin-up and spin-down bands, hence the compound corresponds to the AFM state. Since the energy gaps exist, $La_{1-x}Eu_xGaO_3$ ($x = 0.25$ and 0.5) show insulating characteristics. As x increases further, an internal magnetic field appears and increases gradually since the first and second nearest neighbors are occupied more by magnetic Eu ions. The internal magnetic field produces the exchange split, which results in spin polarization. Spin-up bands cross the Fermi level while spin-down are below (see Figs. 3(d) and 3(e)). As a result, $La_{1-x}Eu_xGaO_3$ ($x > 0.5$) shows a half-metallic FM ground state. As x increases, the substitution of non-magnetic La^{3+} ions by magnetic Eu^{3+} ions drives the system from the insulating state to the half-metallic state.

3.3. Magnetic properties

The total magnetic moments and atom moment for $La_{1-x}Eu_xGaO_3$ are listed in Table 1 and Table 2, respectively. $LaGaO_3$ has no magnetic moment. The magnetic structure of $La_{0.75}Eu_{0.25}GaO_3$ is an AFM state where the moment of Eu_1 is -6.304 μ_B at the site whereas Eu_2 is 6.304 μ_B (see Table 2).

The magnetic structure of $La_{0.5}Eu_{0.5}GaO_3$ is also an AFM state where each moment for Eu ions is aligned antiparallel with the nearest-neighbor one. For $La_{0.25}Eu_{0.75}GaO_3$ and $EuGaO_3$, the FM configuration has the lowest energy and is assumed to be the ground state. The FM state of $EuGaO_3$ is 0.26 eV lower than the G-AFM state. We tested three types of AFM structures of $EuGaO_3$ and found that the G-type AFM is 0.12 eV and 0.30 eV lower than the A-type and C-type AFM, separately.

In the La-rich regime, $La_{1-x}Eu_xGaO_3$ ($0 < x \leq 0.5$) is AFM so that the total magnetic moments (μ_T) equal to 0. As the Eu content keeps increasing, we find a rapid increasing in μ_T. $La_{0.25}Eu_{0.75}GaO_3$ and $EuGaO_3$ have an FM structure. As localized Eu 4f electrons increase, the hybridization of Eu (4f)–O (2p) is strengthened, which strengthens the exchange splitting, and increases the spin magnetization of the system. The increase in the exchange splitting shows Eu doping strengthens the effect of the Stoner mechanism for ferromagnetism in $La_{1-x}Eu_xGaO_3$ ($x > 0.5$), which may lead to a rapid increasing in μ_T. So $La_{1-x}Eu_xGaO_3$ ($x > 0$) compounds change from an AFM state to an FM state with x increasing.

Table 2. The atoms in the parentheses show the sites where La atoms were replaced. The third and last columns show the magnetic moment at various inequivalent sites.

Composition x	Site	Magnetic moment/μB	Composition x	site	Magnetic moment/μB
0	La	0			
0.25	La_1	0	0.75	La_1	0
	Eu_1 (La_2)	–6.304		Eu_1 (La_2)	6.284
	La_3	0		Eu_2 (La_3)	6.281
	La_4	0		Eu_3 (La_4)	6.302
	La_5	0		La_5	0
	Eu_2 (La_6)	6.304		Eu_4 (La_6)	6.248
	La_7	0		Eu_5 (La_7)	6.281
	La_8	0		Eu_6 (La_8)	6.302
0.5	La_1	0	1	Eu_1 (La_2)	6.272
	Eu_1 (La_2)	6.289		Eu_2 (La_1)	6.272
	Eu_2 (La_3)	6.299		Eu_3 (La_3)	6.298
	La_4	0		Eu_4 (La_4)	6.298
	La_5	0		Eu_5 (La_5)	6.272
	Eu_3 (La_6)	–6.289		Eu_6 (La_6)	6.272
	Eu_4 (La_7)	–6.299		Eu_7 (La_7)	6.298
	La_8	0		Eu_8 (La_8)	6.298

4. Conclusions

In short, we studied the electronic structure and magnetic properties of the $La_{1-x}Eu_xGaO_3$ with x of 0, 0.25, 0.5, 0.75, and 1 within the GGA scheme. The crystal structures of the compounds have perovskite structures. The volumes over the range of compounds ($0 \leq x \leq 1$) decrease with increasing x. The calculations results demonstrate that $La_{1-x}Eu_xGaO_3$ is an insulator ground state for the $x = 0$, 0.25 and 0.5 compounds and a half-metallic ground state for the $x > 0.5$ regimes. The magnetic structure for $0 < x \leq 0.5$ is AFM. The magnetic structure for $x > 0.5$ is found to be ferromagnetic. The substitution of non-magnetic La ions by magnetic Eu ions drives

the system from AFM insulator to the FM half metal.

Acknowledgments

We are grateful to the High Performance Computing Center of Nanjing University for the award of CPU hours.

References

[1] Qian J, Zhu Z W, Jiang G S and Liu W 2014 *J. Power Sources* **246** 556
[2] Morales M, Roa J J, Perez-Falcón J M, Moure A, Tartaj J, Espiell F and Segarra M 2014 *J. Power Sources* **246** 918
[3] Hong J E, Ida S and Ishihara T 2014 *J. Power Sources* **259** 282
[4] Wu Y C and Chuang W L 2013 *Int. J. Hydrogen Energy* **38** 12392
[5] Vedat S, Hasan O and Faruk O M 2013 *J. Eur. Ceram. Soc.* **33** 1435
[6] Liu X and Lin J 2006 *J. Appl. Phys.* **100** 124306
[7] Liu X and Lin J 2007 *Appl. Phys. Lett.* **90** 184109
[8] Liu X, Pang R, Quan Z, Yang J and Lin J 2007 *J. Electrochem. Soc.* **154** J185
[9] Liu X and Lin J 2008 *J. Mater. Chem.* **18** 221
[10] Parveen and Gaur N K 2012 *Solid State Sci.* **14** 814
[11] Marti M, Fisher P, Altorfer F, Sheel H J and Tadin M 1994 *J. Phys.: Condens. Matter* **6** 127
[12] Sood K, Singh K and Pandey O P 2014 *J. Renew. Sustain. Energy* **6** 063112
[13] Li Z L, An X Y, Cheng X L, Wang X Mi, Zhang H, Peng L P and Wu W D 2014 *Chin. Phys. B* **23** 037104
[14] Sandeep, Rai D P, Shankar A, Ghimire M P, Sakhya A P, Sinha T P, Khenata R, Omran S B and Thapa R K 2016 *Chin. Phys. B* **25** 067101
[15] Huang C B, Wu H X, Ni Y B, Wang Z Y, Qi M and Zhang C Li 2016 *Chin. Phys. B* **25** 086201
[16] Zhang Y R, Zhang L, Ren J F, Yuan X B and Hu G C 2015 *Acta Phys. Sin.* **64** 178103 (in Chinese)
[17] Wang W H, Zhao G Z and Liang X X 2013 *Chin. Phys. B* **22** 120205
[18] Kresse G and Joubert D 1999 *Phys. Rev. B* **59** 1758
[19] Kresse G and Furthmuller J 1996 *Phys. Rev. B* **54** 11169
[20] Kresse G and Hafner J 1993 *Phys. Rev. B* **47** 558
[21] see http://stokes.byu.edu/findsym.html.
[22] Häussermann U, Blomqvist H and Noréus D 2002 *Inorg. Chem.* **41** 3684
[23] Berkowski M, Fink-Finowicki J, Byszewski P, Diduszko R, Kowalska E, Aleksiyko R, Piekarczyk W, Vasylechko L O, Savytskij D I, Perchuc Â L and KapusAÂniak J 2001 *J. Cryst. Growth* **222** 194
[24] Glowacki M, Runk T, Domukhovski V, Diduszko R, Mirkowsk M, Berkowski M and Dabrowski B 2011 *J. Alloys Compd.* **509** 1756
[25] Knight S K 2012 *J. Solid State Chem.* **194** 286
[26] Dhak P, Pramanik P, Bhattacharya S, Roy A, Achary S N and Tyagi A K 2011 *Phys. Status Solidi B* **248** 1884
[27] Marezio M, Remeika J P and Dernier P D 1968 *Inorg. Chem.* **7** 1337
[28] Denton A R and Ashcroft N W 1991 *Phys. Rev. A* **43** 3161
[29] Alejandro Ŕ, Dillon D F, Jeffrey A E, Serdar O and Peter Z 2013 *Phys. Rev. B* **87** 245117